

Electric field control of the exchange field of a single spin impurity on a surface

Xue Zhang,^{1,2#} Jose Reina-Gálvez,^{3,4#} Di'an Wu,² Jan Martinek,⁵ Andreas J. Heinrich,^{3,6*}
Taeyoung Choi,^{6*} Christoph Wolf^{3,4*}*

1 Spin-X Institute, State Key Laboratory of Luminescent Materials and Devices, Center for
Electron Microscopy, South China University of Technology, Guangzhou 511442, China

2 School of Microelectronics, South China University of Technology, Guangzhou 511442, China

3 Center for Quantum Nanoscience, Institute for Basic Science (IBS), Seoul 03760, Republic of
Korea

4 Ewha Womans University, Seoul 03760, Republic of Korea

5 Institute of Molecular Physics, Polish Academy of Science, Smoluchowskiego 17, 60-179
Poznan, Poland

6 Department of Physics, Ewha Womans University, Seoul 03760, Republic of Korea.

KEYWORDS

scanning tunneling microscopy, electron spin resonance, exchange interaction, electric field,
frequency shifts

ABSTRACT

Electric control of spins offers faster switching and more localized manipulation compared to magnetic fields. In this work, we investigate static electric field effects on electron spin resonance of single molecules and atoms using scanning tunneling microscopy. We observe significant resonance frequency shifts when varying the applied DC voltage. These shifts cannot be adequately explained by g -factor changes or adsorbate displacement. Instead, we propose a model based on the control of the magnetic exchange field exerted to the spin impurity by the static electric field, which accurately reproduces the static electric field dependence of the resonance frequency. Our work provides crucial insights into electric field influence on surface spins, advancing fundamental understanding for many quantum technologies with efficient spin control via electric fields.

INTRODUCTION

The manipulation and control of individual quantum spins on surfaces is critical for advancing quantum information processing and spintronic devices.^{1,2} While oscillating magnetic fields delivered via strip lines have traditionally been used to control the quantum states of spins, electric fields offer significant advantages, including faster switching speeds and more localized application through local gate electrodes.³⁻⁹ This is particularly crucial for quantum computing applications, where rapid gate operations are essential to mitigate decoherence effects. Furthermore, electric field control could lead to more energy-efficient spintronic devices, benefiting low-power, high-density information storage and processing technologies.⁸ Despite these potential advantages, the impact of local electric fields on the quantum properties of surface spins remains poorly understood. To investigate this, the recently developed combination of electron spin resonance (ESR) and scanning tunneling microscopy (STM) can be employed as a

powerful technique. ESR-STM allows for probing and manipulating single atomic and molecular spins with atomic-scale precision and purely by electric fields,¹⁰⁻¹³ making it an ideal tool to study the interplay between electric fields and spin dynamics on surfaces.

In a typical ESR-STM experiment, magnetic impurities are deposited onto a surface and then approached by a magnetic tip. The tip, impurity, and substrate together form a transport junction, and the resulting current can be used to read out the quantum state of the impurity. For simplicity, in this work we assume that the impurity has an electron spin $S = 1/2$, which yields a single electronic transition between the spin-up and spin-down states, $\langle S_z \rangle = \pm 1/2$. The dominant external magnetic field (B_{ext}) aligns the spin $-1/2$ along its direction. The resonance frequency (f_0) is determined by the Zeeman energy, which is set by the sum of the external magnetic field and the effective tip field. When the tip is sufficiently close, the interaction between the spin and the tip is dominated by the exchange interaction. For simplicity, we will ignore long-range dipolar contributions to this interaction. Therefore, the resulting local magnetic field is the sum of the external magnetic field, B_{ext} , and the exchange magnetic field component parallel to the spin set by the tip, $B_{\text{exch}}^{\parallel}$. The sum of these fields determines the Zeeman energy^{14,15} according to Eq. (1):

$$hf_0 = g\mu_B(B_{\text{ext}} + B_{\text{exch}}^{\parallel}), \quad (1)$$

with h being the Planck constant, g being the g -factor and μ_B the Bohr magneton.

Conventionally, the tip height can be used to increase or decrease the exchange contribution to the total magnetic field, as $B_{\text{exch}} \equiv |\vec{B}_{\text{exch}}| \propto \exp(-z/\lambda)$, where z is the tip height and λ is the characteristic decay length of the exchange interaction. Intriguingly, the z -height is not the only way to tune the exchange field \vec{B}_{exch} . Recent studies have reported that changing the applied DC

voltage can yield a shift in f_0 . This was explained by a g -factor dependence on the electric field, $g = g(E)$, where E is the electric field generated by the applied DC voltage across the tip-sample gap.^{16,17} While this model reproduces the experimentally observed frequency shift, it fails to explain how the static electric field modifies the g -factor. A comprehensive model explaining the significant f_0 shift observed experimentally as a function of DC voltage is still lacking.

In this work, we employ ESR-STM to investigate the impact of applied static DC electric fields on the spin resonance of individual molecules and atoms on a surface. We propose a model that explains the frequency shift by an effective exchange field resulting from transport between a spin-polarized electrode and the local spin. Our study elucidates the mechanisms underlying electric field influence on single spins, contributing to the fundamental understanding necessary for developing quantum technologies with fast, local, and energy-efficient spin control.

RESULTS AND DISCUSSION

In our experiment, we utilized two adsorbates, titanium (Ti) atoms and iron(II)-phthalocyanine (FePc) molecules, to investigate the DC electric field effect. Both are known to have electron spin $S = 1/2$ when adsorbed on a bilayer of MgO grown on top of an Ag(100) substrate.^{10,15} FePc molecules, Ti and iron (Fe) atoms were deposited sequentially onto MgO/Ag(100) and then cooled to a cryostat temperature of 2 K in the STM. The metal atoms and molecules are well-isolated from each other, with a low coverage of approximately 0.05 monolayers (ML). The Ti atoms predominantly adsorb on the oxygen-oxygen bridge site in our work and will hereafter be referred to simply as Ti.¹⁸ Fe atoms adsorb exclusively on the oxygen site¹⁴ and exhibit a shorter topographic height than Ti atoms, as shown in Figure 1(a). FePc molecules preferentially adsorb with their central Fe atom located on the oxygen site of the MgO

lattice, with the ligand aligned along the (2, 1) direction relative to the underlying oxygen lattices.^{10,19} We prepare spin-polarized tips by transferring several Fe atoms onto the tip apex with an applied external magnetic field of ~ 0.6 T along the out-of-plane direction.

To perform ESR measurements on Ti and FePc spins, we apply a radio-frequency AC voltage (V_{RF}) to the STM tip, mixing it with the DC voltage (V_{DC}), as illustrated in Figure 1(b). The AC electric field, in combination with a spin-polarized tip, translates into a time-dependent magnetic field that drives spin resonance between ground and excited states.²⁰ Due to the relatively small g -factor anisotropy of Ti and FePc spins which was well characterized previously,^{10,21,22} we can assume that both Ti and FePc spins align with the total magnetic field. The tip field, typically in the order of tens of mT (see Supporting Information), suggests a quantization axis predominantly governed by the external magnetic field. To simplify our discussion, we focus on the case where the external field B_{ext} is applied along the z -direction (B_z) for ESR measurements and the exchange field, parallel to the tip direction, is forming an angle with the external magnetic field. The projection of the exchange field on the spin quantization axis gives $B_{\text{exch}}^{\parallel}$. In this way, as we previously described, the resonance frequency (f_0) of the Ti or FePc spin is determined by the sum of B_z and $B_{\text{exch}}^{\parallel}$ (Eq. (1)).

It is commonly observed that, at a given external magnetic field, f_0 shifts linearly with $B_{\text{exch}}^{\parallel}$, typically achieved by adjusting the tip height via different tunneling parameters.^{15,23} However, we also observed a significant f_0 shift when changing V_{DC} , even with a fixed tip height where $B_{\text{exch}}^{\parallel}$ should remain constant, as shown in the ESR spectra of an individual Ti spin in Figure 1(c). In our approach, we adjust the setpoint current (I_{set}) correspondingly for each V_{DC} to maintain a constant tip-adsorbate distance (d), thereby varying the DC electric field (details are provided in Supporting Information). This method allows ESR measurements with active feedback, preventing

unexpected thermal drift of the tip height. We fitted the ESR spectra with a Lorentzian and extracted f_0 for each V_{DC} applied to Ti, as shown in Figure 1(d). We observed a shift of f_0 towards lower frequencies as $|V_{\text{DC}}|$ increased, corresponding to enhanced out-of-plane DC electric field ($E_z = |V_{\text{DC}}|/d$) acting on the Ti spin. Within the measured V_{DC} range, the total f_0 shift is approximately 150 MHz for Ti.

Previous studies proposed that changes in the g -factor could explain the observed resonance frequency shift.¹⁶ However, our direct measurements of the Ti magnetic moment (μ_{Ti}) under varying DC electric fields (Figure 1(e)) allow us to rule out significant variations of the g -factor. The data reveal that μ_{Ti} remains nearly constant across different V_{DC} values, suggesting that changes in the g -factor contribute minimally to the observed f_0 shift (details of the method for extracting magnetic moments are provided in Supporting Information). To further corroborate these findings, we performed DFT calculations on the g -factors of Ti as a function of applied DC electric field (E_z) (Figure 1(f)). Our calculations show that g_z remains unaffected by E_z , while g_x and g_y exhibit subtle changes at E_z values within our measurement conditions ($|E_z| < 0.2 \text{ V}/0.7 \text{ nm}$).

Our analysis also rules out electric field-induced vertical displacement of the adsorbate as a significant contributor to the observed f_0 shift. By examining the tunneling I - z curve of Ti at various V_{DC} values, we calculated that maintaining a constant f_0 across our V_{DC} range (-200 to -20 mV) would require a tip-adsorbate distance change of approximately 50 pm. This implies an assumed experimental displacement of $\sim 300 \text{ pm}/(\text{V}/0.7 \text{ nm})$. Detailed information of extracting the assumed adsorbate displacement with varied V_{DC} is provided in the Supplementary Information. Such a substantial vertical displacement should be easily detected by STM; yet it was not observed in our experiments. Further supporting this conclusion, our DFT calculations predict

that the mechanical displacement of Ti adsorbed on the MgO surface is only $-0.096 \text{ pm}/(\text{V}/\text{nm})$ when subjected to a DC electric field. This suggests that the electric field has negligible influence on adsorbate position at low V_{DC} . These findings collectively indicate that adsorbate displacement contributes negligibly to the observed f_0 shift.

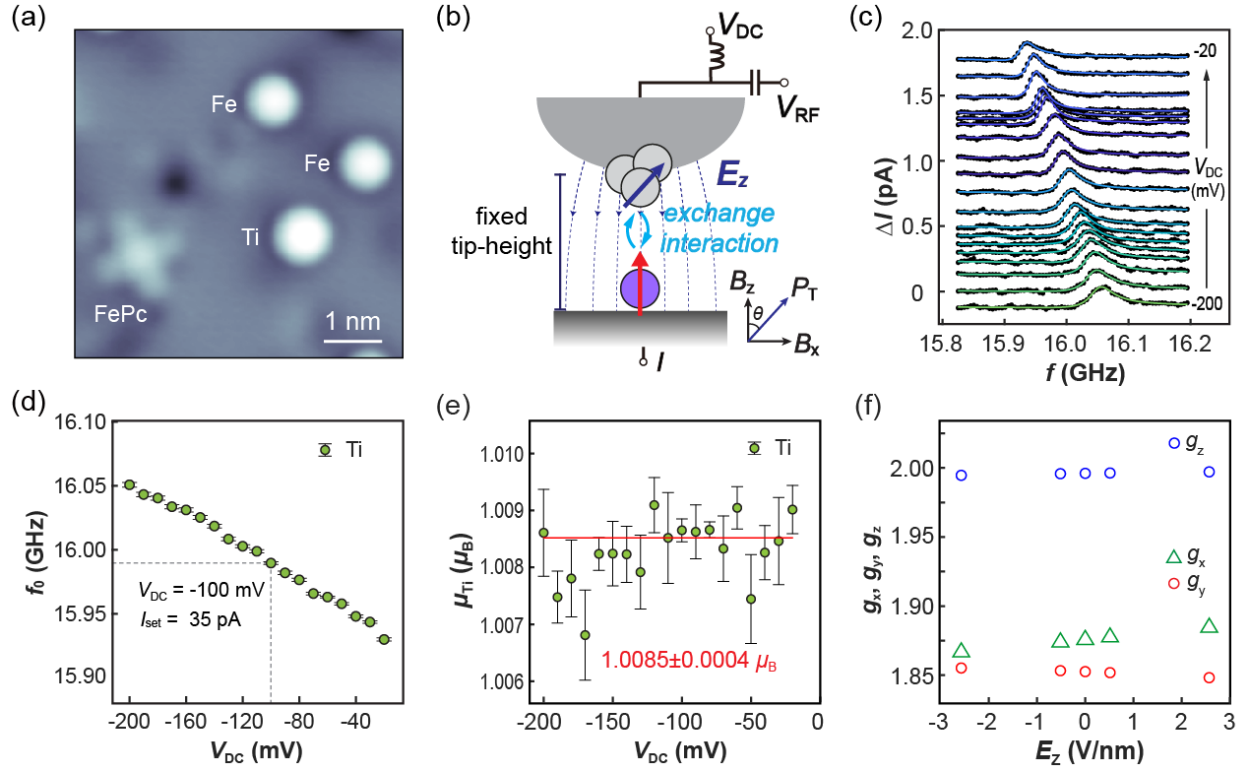


Figure 1. ESR frequency (f_0) shift of a single Ti atom as a function of DC electric field. (a) TM image of the Ti, Fe atoms and the FePc molecule co-adsorbed on the MgO/Ag(100) surface. Scanning parameters: $V_{\text{DC}} = -200 \text{ mV}$, $I_{\text{set}} = 20 \text{ pA}$. (b) Schematic diagram of the ESR set-up at the tunneling junction. P_T is the tip polarization and θ is the angle between the orientation of P_T and the out-of-plane direction. (c) ESR spectra of an individual Ti atom on the bridge binding site measured at varied V_{DC} with fixed tip height. (d) Fitted f_0 at different V_{DC} . The tip height was fixed to be constant by referring to the tunneling parameters of $V_{\text{DC}} = -100 \text{ mV}$, $I_{\text{set}} = 35 \text{ pA}$. (e)

Magnetic moments of the Ti atom measured at different V_{DC} . The red line is the weighted average value of the magnetic moments. ESR conditions: $V_{RF} = 30$ mV, $B_z = 560$ mT, $T = 1.8$ K. (f) Calculated g -tensor elements g_x , g_y , g_z of a Ti atom as a function of the out-of-plane DC electric field (E_z).

To investigate the mechanism behind the V_{DC} -induced shift of the resonance frequency, we conducted comparative ESR measurements on individual FePc molecules under an applied out-of-plane external magnetic field. Figure 2(a) displays the ESR spectra measured at different V_{DC} values with a fixed tip height. We observed a total frequency shift of ~ 300 MHz across the V_{DC} range from -200 to -20 mV (Figure 2(b)), which is larger than that observed for Ti. However, the extracted magnetic moment shows similar consistency across different V_{DC} values (Figure 2(c)). Our calculations of the g -factors for a FePc spin also indicate a weak dependence on the DC electric field along the z -direction (Figure 2(d)), while g_x and g_y only exhibit significant changes at E_z values larger than 2 V/nm, far exceeding our measurement conditions. The calculated mechanical displacement of FePc on MgO is 0.44 pm/(V/nm). However, based on the correlation between tip height and resonance frequency shift at varying V_{DC} , a much larger displacement of ~ 100 pm/(V/0.7 nm) would be required to account for the observed frequency shift (see Supporting Information for details). These findings further support our conclusion that neither g -factor changes nor adsorbate displacement can account for the observed shifts of the resonance frequency.

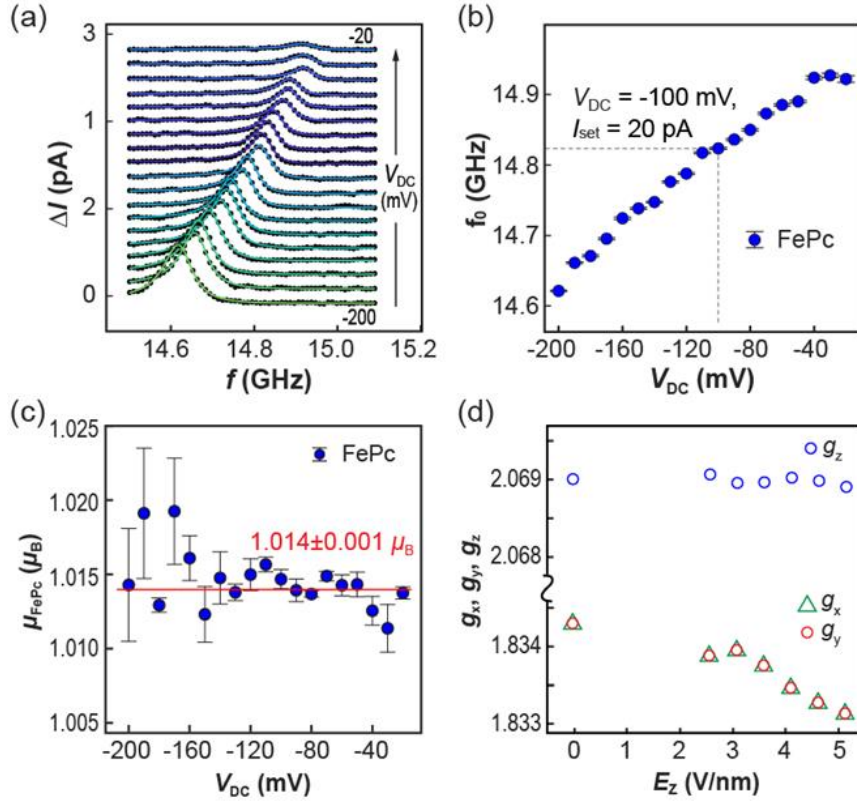


Figure 2. ESR frequency (f_0) shift of an individual FePc molecule as a function of DC electric field. (a) ESR spectra measured at different V_{DC} from -20 mV to -200 mV with fixed tip height. $V_{RF} = 20$ mV, $B_z = 560$ mT, $T = 1.8$ K. (b) Fitted f_0 at different V_{DC} . The tip height was fixed with respect to the tunneling parameters of $V_{DC} = -100$ mV, $I_{set} = 20$ pA. (c) Experimentally measured magnetic moments at different V_{DC} . Red lines give the average value of the magnetic moment of FePc. (d) Dependence of the three components of the g -tensor on an out-of-plane electric field (E_z) for a FePc molecule in vacuum.

Given that changes of the g -factor and vertical displacement are insufficient to explain the significant frequency shift, we propose an alternative explanation. A previous study²⁴ deduced the explicit form of the effective magnetic field from a ferromagnetic electrode, termed the exchange field. This field is influenced by the DC electric field, as adjusting the external DC bias alters the

transport conditions of the tunneling junction. The concept of the exchange field naturally arises from a transport perspective in both the sequential and cotunneling regimes.²⁴⁻²⁶ Its origin lies in many-body effects and is a consequence of the tunneling of electrons through the magnetic impurity.²⁷ It has been successfully applied to quantum dots,^{28,29} where it is also proposed as the origin of the ESR signal.¹³ In the following analysis, we ignore any dipolar contribution of the magnetic tip field, which allows us to present a detailed formulation of the tip (B_{exch}) as follows. The shift of the resonance Δf depends on the exchange field as

$$h\Delta f = hf_0 - g\mu_B B_{\text{ext}} = g\mu_B B_{\text{exch}} \cos \theta = g\mu_B B_{\text{exch}}^{\parallel}, \quad (2)$$

where

$$\vec{B}_{\text{exch}} = -\frac{1}{2\pi} \left[\gamma_T P_T \log \left| \frac{eV_{\text{DC}} - \varepsilon - U}{eV_{\text{DC}} - \varepsilon} \right| \right] \vec{P}_T. \quad (3)$$

Equation (2) introduces an additional complexity by incorporating the angle θ between the tip polarization and the external magnetic field B_{ext} . Therefore, as previously stated, only the projection of the exchange field onto the spin quantization axis contributes to the resonance frequency shift, resulting in the cosine function in Eq. (2). When tip polarization and external field are perpendicular, the projection is zero, causing no resonance frequency shift. Conversely, parallel alignment produces maximum shift but no ESR signal, as both the exchange field and the spin are parallel assuming no local anisotropies preventing the alignment of the spin.^{13,20,30}

We will now discuss the parameters that contribute to the exchange field. Equation (3) encapsulates all relevant transport parameters, primarily depending on the ionization (ε) and charge ($\varepsilon + U$) energies of the Anderson impurity model used to describe the adsorbate, where U is the Coulomb repulsion energy. The impurity model is schematically depicted in Figure 3(a). Here, ε represents the energy required to remove an electron from the impurity, while $\varepsilon + U$ denotes the energy needed to add an electron, both measured relative to the Fermi energy.

Transport mechanisms differ based on bias conditions: at positive DC bias, hole-like transport occurs through an intermediate doubly occupied state; at negative DC bias, electron-like transport proceeds via an intermediate zero-occupation state. At zero DC bias and with $|\varepsilon| = \varepsilon + U$, electron-hole symmetry exists, where electron addition and removal require equal energy, resulting in balanced electron-like and hole-like processes. Note that Eq. 3 assumes negligible Zeeman splitting compared to ionization and charge energies.

The ionization and charge energies determine the strength of the exchange field and the non-linear region of the resonance frequency shift, which is associated with the voltage defined as the difference between the chemical potentials $eV_{\text{DC}} \equiv \mu_{\text{T}} - \mu_{\text{S}}$, at which the exchange field diverges logarithmically. This divergence is mitigated either by electrode-induced broadening^{13,20} or by calculating the Cauchy principal value of the corresponding integral.^{24,25} The finite temperature regime governs both cases, with thermal fluctuations acting as a natural cutoff for the divergence. The exchange field depends exponentially on the tip-adsorbate distance through the coupling parameter $\gamma_{\text{T}} = 2\pi|t_{\text{T}}|^2D_{\text{T}}$, where t_{T} is the tunneling amplitude and D_{T} is the density of states of the tip, assumed to be constant in the so-called wide-band limit approximation. The exchange field does not depend on the coupling to the substrate, γ_{S} , as the substrate is unpolarized. The tip polarization P_{T} affects the exchange field linearly, with zero polarization resulting in no exchange field. This underscores the significant influence of tip polarization on the V_{DC} -induced shift of the resonance frequency. The sign in Eq. (3) indicates ferromagnetic or antiferromagnetic coupling between the tip and magnetic impurity, depending on the product of spin polarization and $\cos \theta$.

Figure 3(b) illustrates a representative example and highlights a crucial aspect of Eq. (3): the electron-hole symmetry point at $eV_{\text{DC}} = \varepsilon + U/2$. At this DC bias, the necessary *additional* energy required to add or remove an electron is equal, and the exchange field vanishes, yielding

the bare resonance energy of the impurity spin under an external magnetic field without additional B-field contributions, such that $hf_0 = g\mu_B B_{\text{ext}}$. This relationship allows us to extract the g -factor for a particular measurement. Notably, these characteristics demonstrate the independence of the exchange field from the tunneling current, as a non-zero net exchange field can exist even at zero DC voltage, provided the electron-hole symmetry point is not at zero V_{DC} .

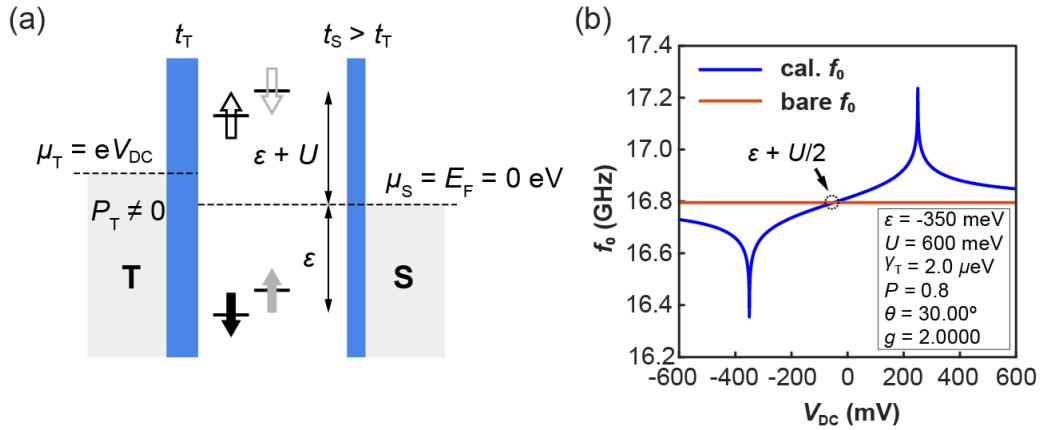


Figure 3. Energy diagram and frequency resonance characteristics in the Single Anderson Impurity Model. (a) Energy level diagram showing the key transport parameters and impurity components that determine the exchange field. The spin impurity splits to two states, \downarrow and \uparrow , separated by the Zeeman energy (black: the ground state, grey: the excited state). The filled arrows represent singly occupied electron states, while the shallow arrows indicate the spin of the hole states. The chemical potential μ_S of the substrate is set to zero, defining the Fermi energy, and the DC bias is applied on the tip. (b) Calculated frequency shift as a function of eV_{DC} . The red curves represent the bare frequencies set by the constant external magnetic field, while the blue curves show the resonance frequencies calculated using Eqs. (2) and (3). The model parameters are displayed in the inset.

The angle θ is crucial in understanding the difference in f_0 shift between in-plane and out-of-plane magnetic fields, as illustrated in Figure 4(a). This data set was obtained on a Ti atom using the same spin-polarized tip and tip-atom distance. Assuming that the polarization of the tip forms an angle θ_x with the B_x direction, this one should form an angle $\theta_z = 90^\circ - \theta_x$ with B_z . This fact allows us to predict the relative orientation of the tip polarization since from Eq. (2) we can write:

$$\tan \theta_x = \frac{g_x(hf_{0z} - g_z\mu_B B_{\text{ext}})}{g_z(hf_{0x} - g_x\mu_B B_{\text{ext}})}. \quad (4)$$

We validated this prediction by fitting our experimental results, using γ_T , ε and U as adjustable parameters. Our observations revealed different slopes in the shift of the resonance frequency of a Ti atom at varying V_{DC} with out-of-plane and in-plane magnetic fields. We achieved good agreement with the theoretical model for an angle of $\theta_x = 30.45^\circ$, obtaining nearly identical adjustable parameters for both data sets, as depicted in Figure 4(a). This consistency across different field orientations strongly supports the validity of our model. However, the uncertainty of the fit is relatively large due to the lack of a strong non-linear regime in the experimental data, as shown in the Supporting Information Figure S5.

The robustness of our model is further demonstrated when analyzing bistable tips with two opposing polarization directions. For simplicity, we assume the same orientation θ_z as previously found, even though it can vary, as introducing this variable parameter would affect the fitted coupling values and complicate the analysis. These tips fluctuate between two magnetic states on a timescale that is fast compared to the signal integration of the ESR-STM.³¹ Consequently, they produce spectra exhibiting two resonances that shift in opposite directions as a function of V_{DC} , as illustrated in Figure 4(b). Our model accounts for this phenomenon by considering both positive and negative spin polarizations P_T , yielding fits that accurately reproduce the inverse signs of the

two curves. The change in the polarization sign can also be interpreted as a rotation of the angle θ_z since maintaining a negative polarization with orientation θ_z is equivalent to having a positive polarization with an orientation of $180^\circ - \theta_z$, as Eqs. (2) and (3) show. Crucially, the intersection of these curves directly reveals the electron-hole symmetry point. This not only aids in fitting the data but also provides a better estimate of the ε and U energies, consistent with the fitting results in Figure 4(a). Moreover, the calculated bare resonance frequency aligns well with this intersection, as shown by the red dashed line in Figure 4(b). This alignment further validates the effectiveness of our theoretical model in explaining the V_{DC} -dependence of the resonance frequency. A list of the best-fit parameters used for the model is given in Figure 4(c). The impurity parameters ε and U are consistent within the fitting uncertainties, with detailed analysis of fit quality and uncertainty range of the fitting parameters provided in Figure S5. Analysis of the four datasets shown in Figure 4 yields average values of $\varepsilon = 330 \pm 18$ meV and $U = 561 \pm 30$ meV. Notably, accurate determination of these parameters requires measurements in the strongly non-linear frequency shift regime, which may be challenging to access due to the low activation barriers for adsorbate hopping and diffusion.

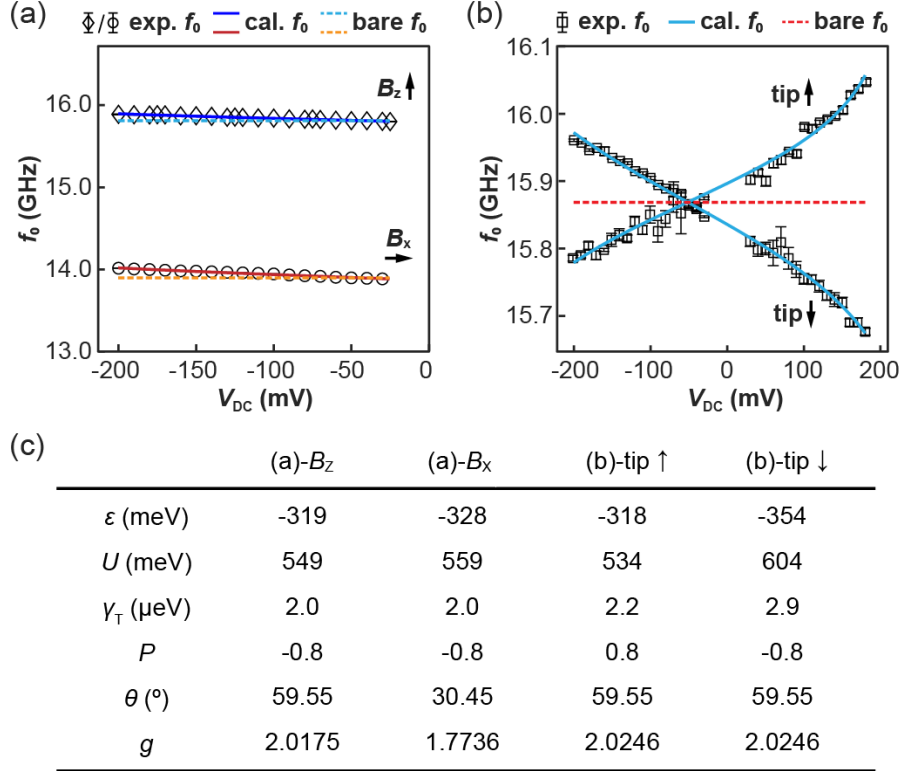


Figure 4. Influence of the external magnetic field and tip polarization on the resonance frequency shift of a Ti atom as a function of V_{DC} . (a) Frequency shifts as a function of V_{DC} with the external magnetic field along the out-of-plane ($B_z = 560$ mT) and in-plane ($B_x = 560$ mT) direction, respectively. The experimentally measured resonance frequencies at different V_{DC} are marked by diamonds and circles while the calculated ones according to Eq. (2) and (3) are plotted by blue and red solid lines. The bare frequencies at different V_{DC} for each field direction are indicated by dashed lines. (b) Experimentally measured (marked by squares) and calculated (solid lines) frequency shift at varied V_{DC} measured by a bistable tip showing two opposite polarization directions (indicated by tip up and tip down) at $B_z = 560$ mT. The tip height at different V_{DC} was fixed by referring to the tunneling condition of (a) $V_{DC} = -100$ mV, $I_{set} = 40$ pA, (b) $V_{DC} = -100$ mV, $I_{set} = 20$ pA. (c) Parameters used for the fits in (a) and (b). ESR parameters: (a) $V_{RF} = 30$ mV, (b) $V_{RF} = 28$ mV.

We can also utilize the exchange field-induced resonance frequency shift to understand the differences between a Ti atom and a FePc molecule. We applied the exchange field model to fit the ESR spectra of Ti and FePc measured with the same spin-polarized tip, as shown in Figure 5(a) and (b), respectively. The model demonstrates good agreement for both species, as summarized in Figure 5(c). For Ti, we obtained γ_T , ε and U values ($\gamma_T = 2.5 \mu\text{eV}$, $\varepsilon = -328 \text{ meV}$, and $U_{\text{Ti}} = 556 \text{ meV}$) similar to those in Figure 4(a-b). However, FePc exhibited a significantly higher Coulomb repulsion $U_{\text{FePc}} = 3863 \text{ meV}$ for a similar ε , meaning it is more difficult to charge the FePc compared to Ti. This indicates a considerably higher charging energy for the molecule, which could be a consequence of FePc on Ag/MgO already being in an anionic state.^{10,32} According to a previous study,¹³ this has direct implications for ESR signal measurement at positive bias, as it predicts lower Rabi rates for large positive voltages compared to negative ones. Interestingly, the best fit of γ_T for FePc is almost five times larger than for Ti. This suggests a closer tip-sample distance for FePc measurements compared to Ti atoms, which aligns with actual experimental conditions.^{10,15,32,33}

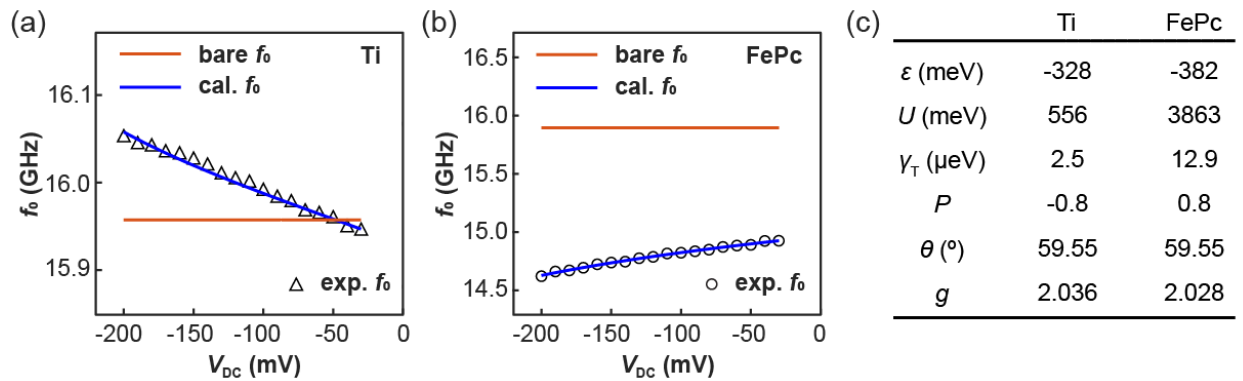


Figure 5. Comparing the V_{DC} -induced frequency shift of Ti and FePc with the same spin-polarized tip. (a) and (b) depict the experimental and calculated resonance frequencies as function

of DC voltage with the same tip for a Ti atom and a FePc molecule, respectively. The black circles and triangles are experimental values extracted from Figures 1 and 2. (c) Fitting parameters used for the Ti and FePc in (a) and (b), respectively.

CONCLUSION

In summary, we investigate the influence of the DC electric field on the electron spin resonance of individual molecules and metal atoms on surfaces. We propose a model based on an exchange field modulated by the DC electric field. A combination of the external magnetic field, the static tip magnetic field, and the exchange field successfully explains the observed shifts of the resonance frequency. This model accounts for various experimental observations, including differences between in-plane and out-of-plane magnetic fields and bistable tip behaviors. Furthermore, our findings demonstrate the potential of utilizing this model as a tool for characterizing the ionization and charging energies of different surface spin species, providing insights into their electronic properties and measurement conditions. Our work enhances the fundamental understanding of electric field effects on surface spins, contributing to the development of quantum technologies with precise spin manipulation based on electric fields.

METHODS

A commercial low-temperature STM system (Unisoku, USM1300) was used for all experiments. Sample preparation involved multiple steps: First, the Ag(100) substrate underwent cycles of Ar⁺ sputtering and annealing to achieve atomically flat terraces. MgO film growth was accomplished by evaporating magnesium onto the clean Ag(100) surface at 400 °C under an oxygen pressure of 1.1×10^{-6} torr. FePc molecules were deposited at room temperature, while Ti

and Fe atoms were deposited onto the cold substrate. All STM and ESR measurements were performed at 2 K with the external magnetic field applied either out-of-plane or in-plane.

The experimental setup for ESR measurements consisted of a signal generator (Keysight, E8257D) providing radio-frequency voltage V_{RF} . DC bias (V_{DC}) was mixed with V_{RF} through a bias tee and applied to the tip. The sample was grounded. For ESR signal detection, V_{RF} was modulated at 95 Hz and measured using lock-in amplification. The tunneling current and ESR signal were detected by an electrometer connected to the sample.

ASSOCIATED CONTENT

Supporting Information.

Extraction of magnetic moments, tip height stabilization at varying DC bias voltages, resonance frequency shift measured with different tips, calculation of the equivalent vertical tip displacement corresponding to resonance frequency shift, discussion on the exchange field model, details of the DFT calculations. (PDF)

AUTHOR INFORMATION

Corresponding Authors

*Xue Zhang - Spin-X Institute, State Key Laboratory of Luminescent Materials and Devices, Center for Electron Microscopy, South China University of Technology, Guangzhou 511442, China; School of Microelectronics, South China University of Technology, Guangzhou 511442, China; orcid.org/0000-0002-4868-3600; *Email*: xuezhang@scut.edu.cn

*Andreas J. Heinrich - *Center for Quantum Nanoscience, Institute for Basic Science (IBS), Seoul 03760, Republic of Korea; Department of Physics, Ewha Womans University, Seoul 03760, Republic of Korea; orcid.org/0000-0001-350 6204-471X; Email: heinrich.andreas@qns.science*

*Taeyoung Choi - *Department of Physics, Ewha Womans University, Seoul 03760, Republic of Korea; orcid.org/0000-0001-5681-807X; Email: tchoi@ewha.ac.kr*

*Christoph Wolf - *Center for Quantum Nanoscience, Institute for Basic Science (IBS), Seoul 03760, Republic of Korea; Ewha Womans University, Seoul 03760, Republic of Korea; orcid.org/0000-0002-9340-9782; Email: wolf.christoph@qns.science*

Author Contributions

#These authors contributed equally. X.Z. and T.C. designed the project. X.Z. performed the experiments. J.R.-G., J.M. and C.W. developed the model and carried out calculations. D.W. analyzed the experimental data. X.Z., J.R.-G. and C.W. wrote the manuscript with the help of all authors. T.C. and A.J.H. advised the project process.

Data availability

All data that support the findings of this study are available in this manuscript and its Supplementary Information, or from the corresponding authors on reasonable request.

Notes

The authors declare no competing interest.

ACKNOWLEDGMENT

All authors acknowledge support from the Institute for Basic Science under grant IBS-R027-D1. X.Z acknowledges financial support from the National Natural Science Foundation of China (grant

agreement No. 22202074) and Science and Technology Project of Guangzhou (grant agreement No. 2023A04J0671). J.M. received support from National Science Centre of Poland (Grant No. 2020/36/C/ST3/00539). We also thank Nicolás Lorente, Soo-hyon Phark, Piotr Kot, Arzhang Ardavan, Piotr Busz, Damian Tomaszewski, Józef Barnaś, Jürgen König for the fruitful discussions.

REFERENCES

- (1) Chen, Y.; Bae, Y.; Heinrich, A. J. Harnessing the quantum behavior of spins on surfaces. *Adv. Mater.* **2023**, *35* (27), 2107534.
- (2) Bi, L.; Liang, K.; Czap, G.; Wang, H.; Yang, K.; Li, S. Recent progress in probing atomic and molecular quantum coherence with scanning tunneling microscopy. *Prog. Surf. Sci.* **2023**, *98* (1), 100696.
- (3) Liu, J.; Mrozek, J.; Ullah, A.; Duan, Y.; Baldoví, J. J.; Coronado, E.; Gaita-Ariño, A.; Ardavan, A. Quantum coherent spin–electric control in a molecular nanomagnet at clock transitions. *Nat. Phys.* **2021**, *17* (11), 1205-1209.
- (4) Gilbert, W.; Tantt, T.; Lim, W. H.; Feng, M.; Huang, J. Y.; Cifuentes, J. D.; Serrano, S.; Mai, P. Y.; Leon, R. C. C.; Escott, C. C.; Itoh, K. M.; Abrosimov, N. V.; Pohl, H.-J.; Thewalt, M. L. W.; Hudson, F. E.; Morello, A.; Laucht, A.; Yang, C. H.; Saraiva, A.; Dzurak, A. S. On-demand electrical control of spin qubits. *Nat. Nanotechnol.* **2023**, *18* (2), 131-136.
- (5) Asaad, S.; Mourik, V.; Joecker, B.; Johnson, M. A. I.; Baczewski, A. D.; Firdausy, H. R.; Mądzik, M. T.; Schmitt, V.; Pla, J. J.; Hudson, F. E.; Itoh, K. M.; McCallum, J. C.; Dzurak, A. S.;

Laucht, A.; Morello, A. Coherent electrical control of a single high-spin nucleus in silicon. *Nature* **2020**, *579* (7798), 205-209.

(6) Pham, V. D.; Ghosh, S.; Joucken, F.; Pelaez-Fernandez, M.; Repain, V.; Chacon, C.; Bellec, A.; Girard, Y.; Sporken, R.; Rousset, S.; Dappe, Y. J.; Narasimhan, S.; Lagoute, J. Selective control of molecule charge state on graphene using tip-induced electric field and nitrogen doping. *npj 2D Mater. Appl.* **2019**, *3* (1), 5.

(7) Hsu, P.-J.; Kubetzka, A.; Finco, A.; Romming, N.; von Bergmann, K.; Wiesendanger, R. Electric-field-driven switching of individual magnetic skyrmions. *Nat. Nanotechnol.* **2016**, *12* (2), 123-126.

(8) Nozaki, T.; Shiota, Y.; Miwa, S.; Murakami, S.; Bonell, F.; Ishibashi, S.; Kubota, H.; Yakushiji, K.; Saruya, T.; Fukushima, A.; Yuasa, S.; Shinjo, T.; Suzuki, Y. Electric-field-induced ferromagnetic resonance excitation in an ultrathin ferromagnetic metal layer. *Nat. Phys.* **2012**, *8* (6), 491-496.

(9) Nowack, K. C.; Koppens, F. H. L.; Nazarov, Y. V.; Vandersypen, L. M. K. Coherent control of a single electron spin with electric fields. *Science* **2007**, *318* (5855), 1430-1433.

(10) Zhang, X.; Wolf, C.; Wang, Y.; Aubin, H.; Bilgeri, T.; Willke, P.; Heinrich, A. J.; Choi, T. Electron spin resonance of single iron phthalocyanine molecules and role of their non-localized spins in magnetic interactions. *Nat. Chem.* **2021**, *14* (1), 59-65.

(11) Wang, Y.; Chen, Y.; Bui, H. T.; Wolf, C.; Haze, M.; Mier, C.; Kim, J.; Choi, D.-J.; Lutz, C. P.; Bae, Y.; Phark, S.-h.; Heinrich, A. J. An atomic-scale multi-qubit platform. *Science* **2023**, *382* (6666), 87-92.

(12) Wang, H.; Fan, P.; Chen, J.; Jiang, L.; Gao, H.-J.; Lado, J. L.; Yang, K. Construction of topological quantum magnets from atomic spins on surfaces. *Nat. Nanotechnol.* **2024**, <https://doi.org/10.1038/s41565-024-01775-2>

(13) Reina-Gálvez, J.; Martinek, J.; Lorente, N.; Wolf, C. In preparation.

(14) Baumann, S.; Paul, W.; Choi, T.; Lutz, C. P.; Ardavan, A.; Heinrich, A. J. Electron paramagnetic resonance of individual atoms on a surface. *Science* **2015**, *350* (6259), 417-420.

(15) Yang, K.; Paul, W.; Natterer, F. D.; Lado, J. L.; Bae, Y.; Willke, P.; Choi, T.; Ferrón, A.; Fernández-Rossier, J.; Heinrich, A. J.; Lutz, C. P. Tuning the exchange bias on a single atom from 1 mT to 10 T. *Phys. Rev. Lett.* **2019**, *122* (22), 227203.

(16) Kot, P.; Ismail, M.; Drost, R.; Siebrecht, J.; Huang, H.; Ast, C. R. Electric control of spin transitions at the atomic scale. *Nat. Comm.* **2023**, *14* (1), 6612.

(17) Kovarik, S.; Schlitz, R.; Vishwakarma, A.; Ruckert, D.; Gambardella, P.; Stepanow, S. Spin torque-driven electron paramagnetic resonance of a single spin in a pentacene molecule. *Science* **2024**, *384* (6702), 1368-1373.

(18) Kim, J.; Noh, K.; Chen, Y.; Donati, F.; Heinrich, A. J.; Wolf, C.; Bae, Y. Anisotropic hyperfine interaction of surface-adsorbed single atoms. *Nano Lett.* **2022**, *22* (23), 9766-9772.

(19) Willke, P.; Bilgeri, T.; Zhang, X.; Wang, Y.; Wolf, C.; Aubin, H.; Heinrich, A.; Choi, T. Coherent spin control of single molecules on a surface. *ACS Nano* **2021**, *15* (11), 17959-17965.

(20) Reina-Gálvez, J.; Wolf, C.; Lorente, N. Many-body nonequilibrium effects in all-electric electron spin resonance. *Phys. Rev. B* **2023**, *107* (23), 235404.

(21) Bae, Y.; Yang, K.; Willke, P.; Choi, T.; Heinrich, A. J.; Lutz, C. P. Enhanced quantum coherence in exchange coupled spins via singlet-triplet transitions. *Sci. Adv.* **2018**, *4* (11), eaau4159.

(22) Kim, J.; Jang, W.-j.; Bui, T. H.; Choi, D.-J.; Wolf, C.; Delgado, F.; Chen, Y.; Krylov, D.; Lee, S.; Yoon, S.; Lutz, C. P.; Heinrich, A. J.; Bae, Y. Spin resonance amplitude and frequency of a single atom on a surface in a vector magnetic field. *Phys. Rev. B* **2021**, *104* (17), 174408.

(23) Willke, P.; Singha, A.; Zhang, X.; Esat, T.; Lutz, C. P.; Heinrich, A. J.; Choi, T. Tuning single-atom electron spin resonance in a vector magnetic field. *Nano Lett.* **2019**, *19* (11), 8201-8206.

(24) Martinek, J.; Sindel, M.; Borda, L.; Barnaś, J.; Bulla, R.; König, J.; Schön, G.; Maekawa, S.; von Delft, J. Gate-controlled spin splitting in quantum dots with ferromagnetic leads in the Kondo regime. *Phys. Rev. B* **2005**, *72* (12), 121302(R).

(25) Busz, P.; Tomaszewski, D.; Barnaś, J.; Martinek, J. Hanle effect in transport through single atoms in spin-polarized STM. *J. Magn. Magn. Mater.* **2023**, *588*, 171465.

(26) Braun, M.; König, J.; Martinek, J. Theory of transport through quantum-dot spin valves in the weak-coupling regime. *Phys. Rev. B* **2004**, *70* (19), 195345.

(27) Weymann, I.; König, J.; Martinek, J.; Barnaś, J.; Schön, G. Tunnel magnetoresistance of quantum dots coupled to ferromagnetic leads in the sequential and cotunneling regimes. *Phys. Rev. B* **2005**, *72* (11), 115334.

(28) Pasupathy, A. N.; Bialczak, R. C.; Martinek, J.; Grose, J. E.; Donev, L. A. K.; McEuen, P. L.; Ralph, D. C. The Kondo Effect in the Presence of Ferromagnetism. *Science* **2004**, *306* (5693), 86-89.

(29) Hauptmann, J. R.; Paaske, J.; Lindelof, P. E. Electric-field-controlled spin reversal in a quantum dot with ferromagnetic contacts. *Nat. Phys.* **2008**, *4* (5), 373-376.

(30) Reina-Gálvez, J.; Lorente, N.; Delgado, F.; Arrachea, L. All-electric electron spin resonance studied by means of Floquet quantum master equations. *Phys. Rev. B* **2021**, *104* (24), 245435.

(31) Yu, J.; Urdaniz, C.; Namgoong, Y.; Wolf, C. On the magnetic bistability of small iron clusters used in scanning tunneling microscopy tip preparation. *New J. Phys.* **2023**, *25* (11), 113035.

(32) Zhang, X.; Reina-Gálvez, J.; Wolf, C.; Wang, Y.; Aubin, H.; Heinrich, A. J.; Choi, T. Influence of the magnetic tip on heterodimers in electron spin resonance combined with scanning tunneling microscopy. *ACS Nano* **2023**, *17* (17), 16935-16942.

(33) Yang, K.; Bae, Y.; Paul, W.; Natterer, F. D.; Willke, P.; Lado, J. L.; Ferrón, A.; Choi, T.; Fernández-Rossier, J.; Heinrich, A. J.; Lutz, C. P. Engineering the eigenstates of coupled spin-1/2 atoms on a surface. *Phys. Rev. Lett.* **2017**, *119* (22), 227206.

Supplementary Information
for

Electric field control of the exchange field of a single spin impurity on a surface

Xue Zhang,^{1,2#} Jose Reina-Gálvez,^{3,4#} Di'an Wu,² Jan Martinek,⁵ Andreas J. Heinrich,^{3,6*} Taeyoung Choi,^{6*} Christoph Wolf^{3,4*}*

1 Spin-X Institute, State Key Laboratory of Luminescent Materials and Devices, Center for Electron Microscopy, South China University of Technology, Guangzhou 511442, China

2 School of Microelectronics, South China University of Technology, Guangzhou 511442, China

3 Center for Quantum Nanoscience, Institute for Basic Science (IBS), Seoul 03760, Republic of Korea

4 Ewha Womans University, Seoul 03760, Republic of Korea

5 Institute of Molecular Physics, Polish Academy of Science, Smoluchowskiego 17, 60-179 Poznan, Poland

6 Department of Physics, Ewha Womans University, Seoul 03760, Republic of Korea

Table of Contents

1. Extraction of magnetic moments from ESR measurement at different tunneling currents
2. Fixing the tip height to measure ESR spectrum at different DC voltage
3. Electric field influence on the resonance frequency measured with different tips
4. Calculation of the equivalent vertical tip displacement corresponding to resonance frequency shift
5. Discussion on the exchange field model
6. Details of the DFT calculations

1. Extraction of magnetic moments from ESR measurement at different tunneling currents

The magnetic tip with a few Fe atoms at the apex is supposed to be interacting with the magnetic adsorbate in manner of exchange and dipolar coupling, where the former one is dominant. This interaction can be simplified as an effective tip field (B_{exch}) exerted on the magnetic adsorbate. When the exchange interaction between the tip and the adsorbate dominates, which is the common case in an STM-ESR experiment, the strength of the interaction is exponentially determined by the tip-adsorbate distance. Consequently, the tip field can be approximated to be proportionally changed with the tunneling current. Given the much larger external magnetic field along the out-of-plane direction utilized in our work compared to the relatively small tip field, we denote the external magnetic field as B_z , the total tip field component projected to the z-direction as B_{exch} (which is in an order of tens of mT here). Both FePc molecule and Ti atom on MgO/Ag surface are found to be $S = 1/2$ system, based on which we can consider the FePc and Ti spin following the direction of the total magnetic field ($B_z + B_{exch}$). Thus, in the ESR measurement of an individual FePc and Ti, the resonance frequency (f_0) is determined solely by the external magnetic field and tip field due to Zeeman interaction, as described by Eq. (1) in the main text.

According to Eq. (1), we can characterize the relative direction of B_{exch} with respect to B_z by tracking the shift of f_0 with varied current, as shown in Figure S1(a) and (d). For the tip used to measure Ti and FePc in Figs. 1 and 2, f_0 shifts linearly to lower and higher frequency, respectively, with increased current when the external magnetic field is kept constant (Figure S1(a) and (d)), indicating B_z and B_{exch} have opposite/same sign and the alignment between tip field and the local spin is antiferromagnetic (AFM)/ ferromagnetic (FM). By fitting the linear shift of f_0 as a function of I_{set} and extrapolating to $I_{set} = 0$ ($B_{exch} = 0$) (Figure S1(b) and (e)), the intersection with the frequency axis (f'_0) gives the magnetic moment of FePc: $\mu_{FePc} = \frac{hf'_0}{2B_z}$. The effective tip fields at different current setpoints are plotted in Figure S1(c) and (d).

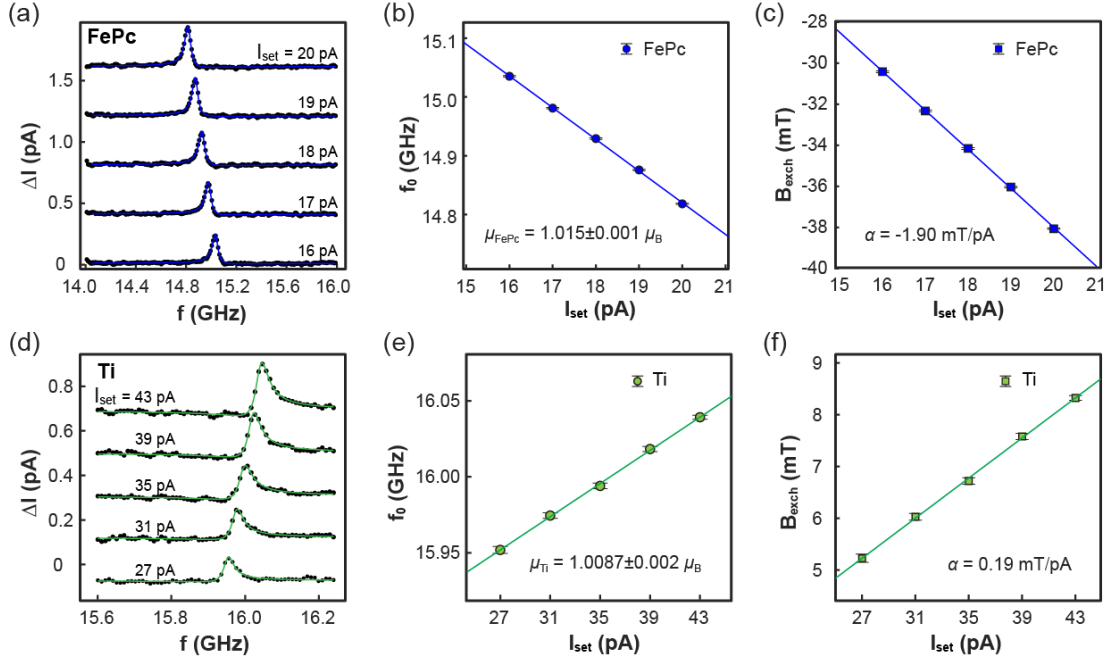


Figure S1. Extraction of magnetic moment from current-dependent ESR measurements. (a)(d) Measured and fitted ESR spectra of an individual FePc molecule and a Ti atom, respectively, with varied current by using the same tip as Figs. 1 and 2. ESR conditions: $B_z = 560$ mT, $V_{DC} = -100$ mV, (a) $V_{RF} = 20$ mV and (d) $V_{RF} = 35$ mV. Each spectrum has been vertically shifted by 0.4 pA in (a) and 0.2 pA in (d) from another. (b)(e) Fitted resonance frequency (f_0) as a function of current (I_{set}) for FePc and Ti from the spectra in (a) and (d). The magnetic moment of FePc and Ti was extracted by extrapolating to zero-current region according to Eq. (1). (c)(f) Corresponding tip field at different current setpoints used in (a) and (d), varying linearly as the current with a pre-factor α .

2. Fixing the tip height to measure ESR spectrum at different DC voltage

In the main text, we showed series of ESR spectra measured in different dc electric field by varying the dc bias while keeping the tip height (tip-sample distance) unchanged. To do this, the referential tip height was decided before performing ESR measurement and corresponding setpoint current (I_{set}) was measured at different dc bias (V_{DC}) when tip height was kept the same. Notably, I_{set} is always recorded as positive value due to the default settings of the scanning software, while in the real measurement I_{set} is automatically converted to have a negative sign when $V_{DC} < 0$ (e.g. I - z curve shown in Figure S4). Then the ESR spectrum was taken with the V_{DC} and I_{set} determined above. During each ESR measurement, feedback was on but with very low gain to guarantee

the constant tip height. Figure S2 shows the corresponding I_{set} at different V_{DC} with same tip height on FePc and Ti, respectively. Due to the different conductance of FePc and Ti, the absolute tip height with respect to the surface is different for FePc and Ti under the same tunneling conditions. The tip is supposed to be $\sim 1 \text{ \AA}$ closer to the surface in FePc case compared to Ti according to the STM topography shown in Figure 1(a) with comparable tunneling parameters.

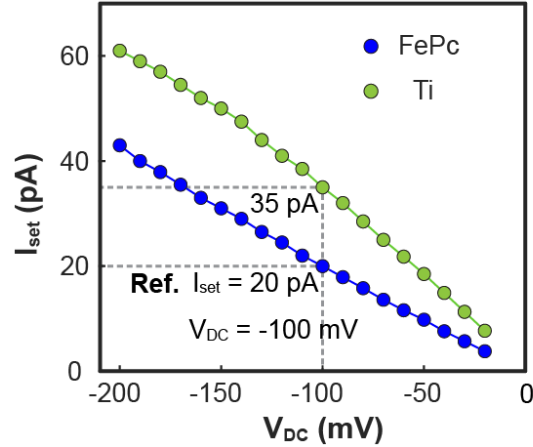


Figure S2. V_{DC} and corresponding I_{set} used for the ESR measurements shown in Figures 1 and 2. The referential tip height was chosen when the tunneling parameters were set as $V_{DC} = -100\text{mV}$, $I_{set} = 20 \text{ pA}$ for FePc and $V_{DC} = -100\text{mV}$, $I_{set} = 35 \text{ pA}$ for Ti.

3. Electric field influence on the resonance frequency measured with different tips

To clarify the electric field influence on the resonance frequency of FePc and Ti, we prepared different spin-polarized tips and measured the ESR spectra at varied V_{DC} with fixed tip height, as shown in Figure S3. The slope and direction of f_0 shift as a function of V_{DC} shows tip dependence, which can be attributed to the difference in the tip polarization as discussed in the main text.

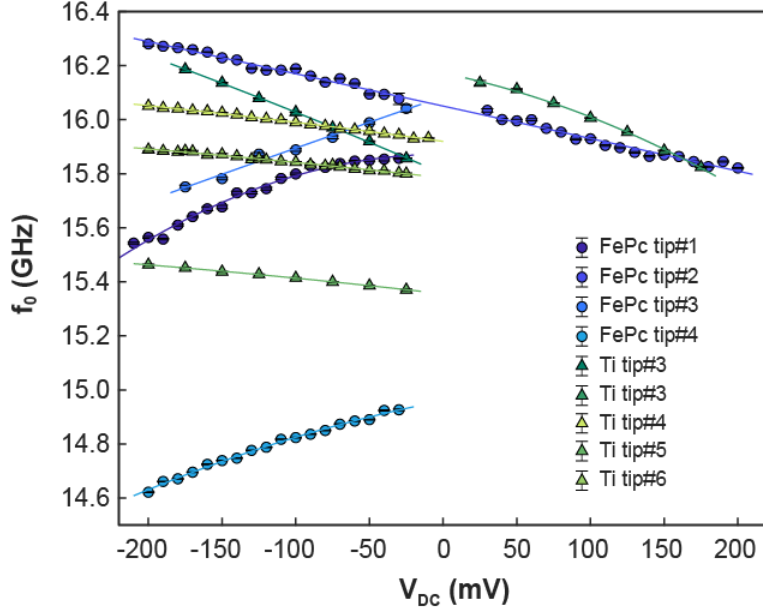


Figure S3. Electric field influence on the resonance frequency of FePc and Ti measured with different tips.

4. Calculation of the equivalent vertical tip displacement corresponding to resonance frequency shift

We measured the vertical displacement of an individual FePc molecule and Ti atom in varied DC electric fields in an indirect way. We combined the f_0 -shift in ESR with the I - z characteristic feature of the tunneling junction. Given the hypothesis of molecular/atomic displacement induced by a dc electric field, the distance between the tip and the adsorbate varies correspondingly when the tip height is kept constant with respect to the surface. As a result, the interaction between the tip and the adsorbate varies and yields a change in B_{exch} , which in the end shifts f_0 according to Eq. (2). However, we note that the shift in f_0 shown in Figure 1(d) and (e) can be compensated by adjusting the setpoint current since we observed a linear variation of $f_0(B_{tip})$ as a function of I_{set} at fixed V_{DC} (Figure S1). Thus, the compensate current (I_{comp}) can be expressed as $I_{comp} = \frac{\Delta f_0}{\alpha}$, where Δf_0 is the resonance frequency shift with respect to a reference and α is the linear coefficient extracted from f_0 vs. I_{set} at a given V_{DC} . Figure S4(a) and (d) show the I_{comp} for FePc and Ti, respectively, at each V_{DC} by comparing to the referential f_0 set at $V_{DC} = -100$ mV, $I_{set} = 20$ pA. As discussed above, I_{comp} is directly related to the change in the tip-adsorbate distance and is realized by adjusting the vertical tip movement. Eventually, the amount of tip displacement needed to maintain constant tip-

adsorbate distance (i.e. B_{tip}) is equal to that of the adsorbate displacement when the tip height is constant at a given dc electric field. To convert I_{comp} into the change in distance, we performed I - z spectroscopy at different V_{DC} on FePc and Ti (Figure S4(b) and (e)) respectively and then extracted the amount of tip movement (Δz) that corresponds to each I_{comp} , as shown in Figure S4(c) and (f). $\Delta z > 0$ means the tip has to move out for compensation (adsorbate displaces closer to the tip) while $\Delta z < 0$ means tip moving in (adsorbate displaces further from the tip). We found Δz for both FePc and Ti changes linearly as V_{DC} .

Based on above discussions, under our experiment conditions, the change in the resonance frequency of ESR spectrum is linearly related to the current at given dc bias ($f_0 = \alpha \cdot I + \beta$). Thus, the shift of resonance frequency (Δf_0) compared to a referential one can be compensated by adjusting the current by $I_{comp} = \frac{\Delta f_0}{\alpha}$ accordingly. Then we measured the I - z curve at different V_{DC} passing through the referential tip height ($\Delta z = 0$) on FePc and Ti, respectively, as shown in Figure S4(b) and (e). During the I - z measurement, the feedback is off and tip moves in ($\Delta z < 0$) or out ($\Delta z > 0$) starting from the referential tip height. Given the small amount of tip movement (tens of pm), we can fit the I - z curve with a polynomial function to well reproduce the exponential decrease of current as the tip-sample distance gets larger. Utilizing the fitted I - Δz expression, we can convert the I_{comp} obtained at different V_{DC} to corresponding displacement that the tip has to move, as displayed in Figure S4(c) and (f). The Δz needed to correct the shift of f_0 is supposed to represent the change in the tip-adsorbate distance due to the mechanical displacement of the magnetic adsorbate induced by dc electric field.)

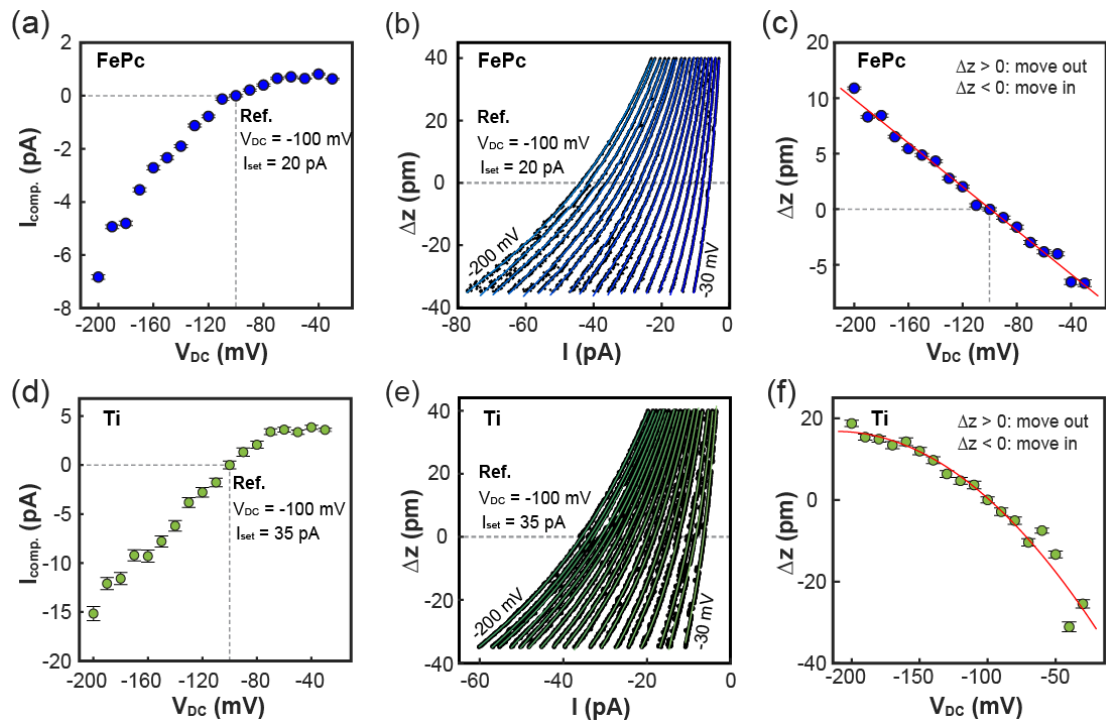


Figure S4. Conversion from resonance frequency shift to tip height compensation. (a)(d) Compensate current (I_{comp}) which is required adding to the setpoint current at different V_{DC} to tune f_0 same as the referential one for FePc and Ti, respectively. I_{comp} of the referential f_0 obtained at $V_{DC} = 100$ mV, $I_{set} = 20$ pA is set as 0. (b)(e) I - z curves measured on (b) FePc and (e) Ti at different V_{DC} . $\Delta z = 0$ was set by referring to the tip height with tunneling parameters of $V_{DC} = -100$ mV, $I_{set} = 20$ pA on FePc and $V_{DC} = -100$ mV, $I_{set} = 35$ pA on Ti. $\Delta z > 0$: tip moves out compared to the referential tip height. $\Delta z < 0$: tip moves in compared to the referential tip height. The colored lines are fits of the I - z data points using 3-order polynomial function as a good approximation of exponential function when Δz is small. (c)(f) Converted displacement of the tip height (Δz) that needed to compensate for the shift in f_0 compared to the referential one. Δz of the referential point is set as 0. $\Delta z > 0$ means the tip has to be moved out and vice versa.

5. Discussion on the exchange field model

Equation 3 in the main text corresponds to the low temperature limit, meaning that $k_B T \ll |\varepsilon|, \varepsilon + U$. A more general formula expression would be:

$$\vec{B}_{exch} = -\frac{1}{\pi} \gamma_T P_T \int d\omega \left[\frac{f_T(\omega)}{\omega - \varepsilon - U} + \frac{1 - f_T(\omega)}{\omega - \varepsilon} \right] \vec{P}_T, \quad (S1)$$

where the bias DC voltage $eV_{DC} = \mu_T$ and the temperature $k_B T$ enters via the Fermi function. From a physical perspective, Equation S1 can be interpreted in terms of two

distinct quantum fluctuations: the first term describes hole-like processes, while the second term represents particle-like processes. The integration captures contributions from a broad electron energy range (beyond $k_B T$), highlighting the many-body nature of the exchange field, which transcends the single-electron picture of the sequential tunneling regime. This is further illustrated by the fact that the exchange field vanishes if Coulomb repulsion is absent.

Let us now examine the fitting results in greater detail. It is important to note that the results presented in the main text exhibit significant uncertainties. These arise from the limited number of data points in the non-linear region of the exchange field and the lack of a well-defined electron-hole symmetry point. These uncertainties can reach up to 50% of the fitted values, with the smallest ones corresponding to the bistable tip data and the FePc case from the main text, for the reasons explained earlier. Computing the residual (R) allows us to visualize how reliable the fitting is for a fixed coupling to the tip. This is shown in Figure S5 as a 2D color plot, where we explore the values of ϵ and U within the range indicated by the uncertainties of the fit. For FePc (Figure S5(a)), since the data shows some non-linearity, the fitting provides a smaller range compared to that of the Ti (Figure S5(b)) with the same tip. There, we find a noticeable increase in the area with a residual lower than 50 MHz, larger values are considered significant due to the high accuracy in determining the resonance position in the experiments. This indicates that, despite the large uncertainties, the fitting is sufficiently reliable since the region with a low residual is small enough and well-defined. Figure S5(c) and (d) include residuals for the bistable tip data set. Here, the value range is minimal for the reasons previously discussed, and we can clearly identify the region with the lowest residual, further demonstrating the reliability of the fit. The impurity parameters ϵ and U remain consistent within fitting uncertainties, as stated in the main text. Figure S6 illustrates this by mirroring the fitting values of the bistable tip data about the bare frequency, revealing good overlap between original and mirrored curves. This symmetry demonstrates that inverting the tip spin polarization leads to an exact reversal in resonance frequency shifts.

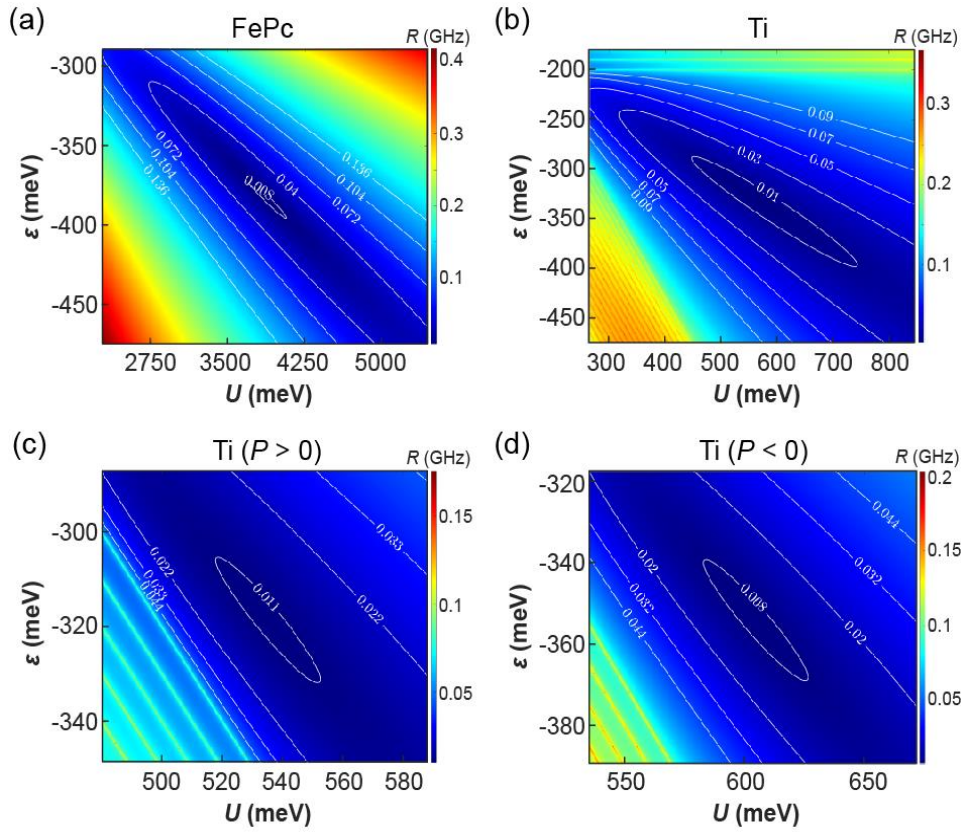


Figure S5. Uncertainty of the fitting parameters in the exchange field model. (a)(b) Residual of the fitting for FePc and Ti, respectively, measured with the same tip as a function of the ionization energy and Coulomb repulsion, ε and U , shown in a 2D color plot. Both plots show an identifiable region where the residual is sufficiently low to ensure the accuracy of the fitting (< 50 MHz), which is lower than the actual fitting error. In the case of FePc, this region is smaller than that of Ti. (c) and (d) show the residual for the data set of the bistable tip where the uncertainty of the fitting is the lowest, although the region with a sufficiently small residual is similar in size to that of (c). Fitting parameters are detailed in Figures 4 and 5 of the main text.

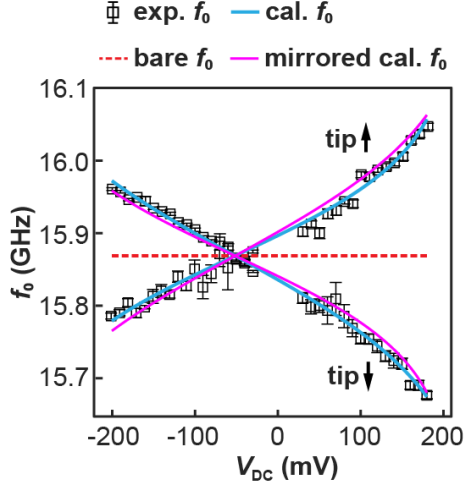


Figure S6. Comparison between original and mirrored fitting values for the bistable tip case.

6. Details of the DFT calculations

We performed DFT calculations using Quantum Espresso (V 7.0 and newer)^{1,2} in line with our previous works on Ti and FePc on 2 ML of MgO on silver.³⁻⁵ In short, FePc and Ti were relaxed according to the described adsorption site (see main text) on 2 ML of MgO with the lowest layers frozen. We built lateral supercells that ensured a separation of the adsorbates by 7 Å (FePc) and 12 Å (Ti) and padded by 10 Å of vacuum in z-direction. Pseudopotentials from the PSLibrary⁶ were used to describe the atomic species with a cutoff of 70 Ry for the wave functions and a dual of 8. For the exchange correlation approximation, we used GGA-PBE.⁷ To calculate the replacement under a static external electric field we relaxed the full system for every value of the field. To calculate the g-factor modulation as a function of the external static electric field we used GIPAW.⁸ An example configuration of each system is shown in Figure S7.

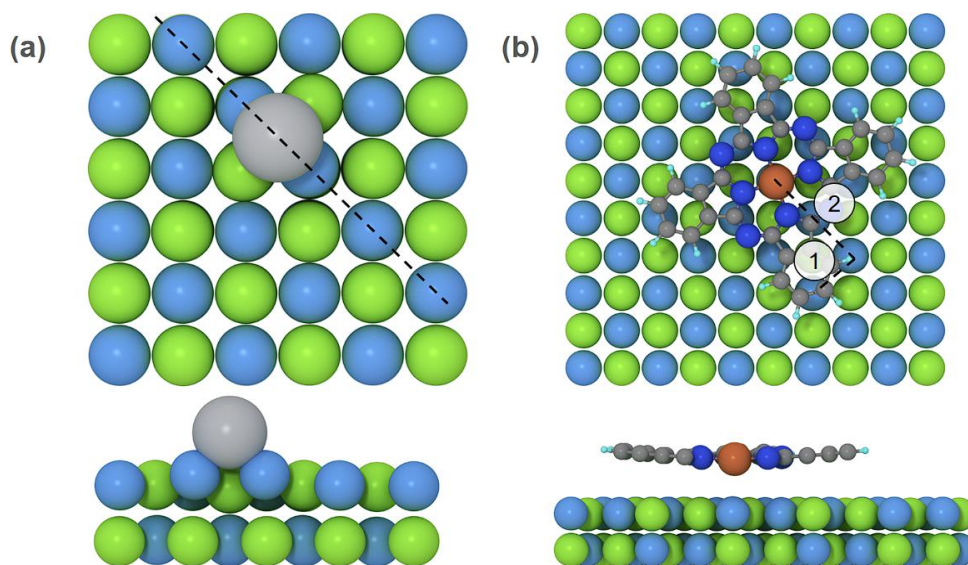


Figure S7. Example configuration of (a) Ti adsorbed on a bridge site and (b) FePc adsorbed in (2,1) ligand configuration. Side views are not drawn at the same scale and are just used to show the adsorption geometry.

REFERENCES

- [1] P. Giannozzi et al., QUANTUM ESPRESSO: a modular and open-source software project for quantum simulations of materials. *J. Phys.: Condens. Matter* **2009**, *21* (39), 395502.
- [2] P. Giannozzi et al., Advanced capabilities for materials modelling with Quantum ESPRESSO. *J. Phys.: Condens. Matter* **2017**, *29* (46), 465901.
- [3] Zhang, X.; Wolf, C.; Wang, Y.; Aubin, H.; Bilgeri, T.; Willke, P.; Heinrich, A. J.; Choi, T., Electron spin resonance of single iron phthalocyanine molecules and role of their non-localized spins in magnetic interactions. *Nat. Chem.* **2021**, *14* (1), 59-65.
- [4] Kim, J.; Jang, W.-j.; Bui, T. H.; Choi, D.-J.; Wolf, C.; Delgado, F.; Chen, Y.; Krylov, D.; Lee, S.; Yoon, S.; Lutz, C. P.; Heinrich, A. J.; Bae, Y., Spin resonance amplitude and frequency of a single atom on a surface in a vector magnetic field. *Phys. Rev. B* **2021**, *104* (17), 174408.
- [5] Willke, P.; Bae, Y.; Yang, K.; Lado, J. L.; Ferrón, A.; Choi, T.; Ardavan, A.; Fernández-Rossier, J.; Heinrich, A. J.; Lutz, C. P., Hyperfine interaction of individual atoms on a surface. *Science* **2018**, *362* (6412), 336-339.
- [6] Dal Corso, A., Pseudopotentials periodic table: From H to Pu. *Comput. Mater. Sci.* **2014**, *95*, 337-350.

- [7] Perdew, J. P.; Burke, K.; Ernzerhof, M., Generalized Gradient Approximation Made Simple. *Phys. Rev. Lett.* **1996**, *77* (18), 3865-3868.
- [8] Varini, N.; Ceresoli, D.; Martin-Samos, L.; Girotto, I.; Cavazzoni, C., Enhancement of DFT-calculations at petascale: Nuclear Magnetic Resonance, Hybrid Density Functional Theory and Car–Parrinello calculations. *Comput. Phys. Commun.* **2013**, *184* (8), 1827-1833.